Effect of Added Poly(oxyethylene)dodecyl Ether on the Phase and Rheological Behavior of Wormlike Micelles in Aqueous SDS Solutions

Durga P. Acharya,*,† Takaaki Sato,‡ Masaya Kaneko,† Yashveer Singh,§ and Hironobu Kunieda†

Graduate School of Environment and Information Sciences, Yokohama National University, Tokiwadai 79-7, Hodogaya-ku, Yokohama 240-8501, Japan, Division of Physics and Applied Physics, Faculty of Science and Engineering, Waseda University, Okubo 3-4-1, Shinjuku-ku, Tokyo 169-8555, Japan, and PANalytical Asia Pacific, Spectris Pte Ltd, No. 31 Kaki Bukit Road 3, #06-04105 Techlink, Singapore 417818

Received: August 17, 2005; In Final Form: November 2, 2005

Upon the addition of a short EO chain nonionic surfactant, poly(oxyethylene) dodecyl ether ($C_{12}EO_n$), to dilute micellar solution of sodium dodecyl sulfate (SDS) above a particular concentration, a sharp increase in viscosity occurs and a highly viscoelastic micellar solution is formed. The oscillatory-shear rheological behavior of the viscoselastic solutions can be described by the Maxwell model at low shear frequency and combined Maxwell−Rouse model at high shear frequency. This property is typical of wormlike micelles entangled to form a transient network. It is found that when $C_{12}EO_4$ in the mixed system is replaced by $C_{12}EO_3$ the micellar growth occurs more effectively. However, with the further decrease in EO chain length, phase separation occurs before a viscoelastic solution is formed. As a result, the maximum zero-shear viscosity is observed at an appropriate mixing fraction of surfactant in the SDS−$C_{12}EO_3$ system. We also investigated the micellar growth in the mixed surfactant systems by means of small-angle X-ray scattering (SAXS). It was found from the SAXS data that the one-dimensional growth of micelles was obtained in all the SDS−$C_{12}EO_n$ ($n = 0-4$) aqueous solutions. In a short EO chain $C_{12}EO_n$ system, the micelles grow faster at a low mixing fraction of nonionic surfactant.

Introduction

When a hydrophilic surfactant is dissolved in water, in most cases, spherical or sphere-like aggregates or micelles are formed. Due to small and sphere-like micelle formation, most of the aqueous surfactant solutions have low viscosity and Newtonian flow is observed. However, under certain conditions (adding salt or combining cationic or anionic surfactants, etc.), one-dimensional (1D) growth of micelles takes place and long, flexible aggregates called wormlike or threadlike micelles are produced.[1−9] Due to entanglement of the wormlike micelles, their aqueous systems show highly viscoelastic behavior. Although the formation of wormlike micelles has been reported in aqueous nonionic surfactant solutions,[10,11] the highly viscoelastic solutions were mainly investigated in cationic and/or cationic−anionic surfactant systems, often in the presence of inorganic or organic salts. Recently, it was reported that a viscoelastic micellar solution of wormlike micelles is formed in the salt-free condition when a lipophilic nonionic surfactant such as short hydrophilic chain poly(oxyethylene) alkyl ether or alkanolamide is added to the dilute micellar solution of hydrophilic cationic, anionic, or nonionic surfactants.[12−17] However, direct structural evidence on the elongation of micelles has not been fully studied in the mixed surfactant systems.

The micellar growth induced by lipophilic nonionic amphiphiles is attributed to the decrease in an average cross-sectional area per surfactant and increases the aggregation number of the aggregate. Since the radius of the spherical aggregate cannot exceed the length of the fully extended lipophilic chain, there should be a limit of upper aggregation number for the spherical aggregate. Due to this packing constraint, a change in micellar shape, such as a sphere−rod transition, is usually observed with the successive addition of the nonionic amphiphile.

Size of the head and tail group of the lipophilic surfactant is one of the factors that affects the micellar growth and the rheological behavior of the solution.[12−14,16,17] For hexadecyltrimethylammonium bromide (CTAB), gemini, and sucrose alkanoate surfactant systems, $C_{12}EO_3$ is the most efficient to increase the viscosity of the solutions.[13,18,19] If the shorter EO chain $C_{12}EO_n$ is added, then phase separation takes place before increasing viscosity. On the other hand, if a longer EO or more hydrophilic surfactant is employed, the micellar growth is not sufficient to form aqueous viscoelastic solutions. Hence, only a decrease in the average occupied area is not enough to form long and flexible wormlike micelles.

In this context, we report the phase behavior of SDS−$C_{12}EO_n$ systems in a water-rich region and variation of rheological behavior of the wormlike micellar solutions. Additionally, the mechanisms of micellar growth were investigated by means of small-angle X-ray scattering (SAXS).

Experimental Section

Materials. Sodium dodecylsulfate (SDS, purity > 99%) was obtained from Aldrich Chemicals. Homogeneous poly(oxyethylene) dodecyl ethers, abbreviated as $C_{12}EO_n$; $n = 1-4$, where

* To whom correspondence should be addressed. E-mail: acharya@ynu.ac.jp. Tel and Fax: +81-45-339-4190.
† Yokohama National University.
‡ Waseda University.
§ PANalytical Asia Pacific.

10.1021/jp054631x CCC: $33.50 © 2006 American Chemical Society
Published on Web 12/18/2005

EO stands for the oxyethylene unit, were the product of Nikko Chemical Co. Guaranteed-grade dodecanol ($C_{12}EO_0$) was purchased from Tokyo Kasei Kogyo Co. Ltd. All the chemicals were used as received for phase study and rheological measurement. SDS contains a trace of impurity, mainly unreacted alcochol, which may largely influence its self-organization in aqueous media. Hence, SDS was recrystallized in ethanol three times, and this sample was used for the determination of micellar structure by SAXS, especially, in the absence of $C_{12}EO_n$ or in the presence of a small amount of the cosurfactant. The surface tension minima in the surface tension−concentration curve disappeared in this purified SDS aqueous solution.

Phase Diagram. For the study of phase behavior, sealed ampules containing the required amount of reagents were homogenized and kept in a water bath at 25 °C from a few days (micellar samples) to several weeks (liquid-crystals samples) for equilibration. The liquid-crystal phases were identified by polarizing microscopy and from SAXS.

Rheological Measurements. The samples of $C_{12}EO_n$/SDS solutions for rheological measurements were prepared by adding the required amount of $C_{12}EO_n$ to 0.15 M (4.32 wt %) SDS. These samples were homogenized and kept in a water bath at 25 °C for at least 24 h to ensure equilibration before performing the measurements. The rheological measurements were performed in an ARES rheometer (Rheometric Scientific) at 25 °C using a couette (diameter 34 mm and bob length 33 mm) for low viscosity solutions and cone-plate geometry (diameter 25 mm and cone angle 0.04 rad) for highly viscous gels. Frequency sweep measurements were performed in the linear viscoelastic regime of the samples, as determined previously by dynamic strain sweep measurements.

SAXS Measurements. The identification of liquid-crystalline phases was done by SAXS using a *Nanoviewer* instrument (Rigaku Corporation, Japan), operated at 40 kV and 20 mA power beam and equipped with a CCD camera as the detector. Samples were placed in the sample holder and sealed by a plastic film (Mylar method).

SAXS measurements on 0.15 M aqueous SDS and SDS/$C_{12}EO_n$ micellar solutions were performed by the use of a SAXSess camera (Anton Paar, PANalytical) equipped with the PW3830 laboratory X-ray generator with a long-fine focus sealed glass X-ray tube (Kα wavelength of $\lambda = 0.1542$ nm) from PANalytical, focusing multiplayer optics, a block collimator for slit collimation, a translucent beam stop, an image plate (IP) detector, and a temperature-controlled sample holder unit (TCS 120). The apparatus was operated at 40 kV and 50 mA. The sample was taken in a clean capillary, and the same capillary was repeatedly used for all measurements. The scattered intensity recorded on the IP was read by means of a Cyclone storage phosphor system (Perkin-Elmer, U.S.A.). Because of the transluscent beam stop, the raw scattering data always include a reduced primary intensity at a scattering vector $q = 0$. All the data were normalized to the same incident primary-beam intensity for the transmission calibration and were corrected for the background scattering from the capillary and the solvent. The maximum resolution of the measurement, or q_{min}, was ∼0.08 nm^{-1}, which corresponds to ∼40 nm and ∼80 nm as detectable maximum size for a particle and interlayer spacing, respectively.

When the system is sufficiently dilute, so that the effect of the interparticle interference scattering, that is, the structure factor $S(q) \sim 1$, the spatially averaged q-dependent scattering intensity, $I(q)$, is given by

$$I(q) = 4\pi \int_0^\infty p(r) \frac{\sin qr}{qr} \mathrm{d}r \quad (1)$$

where $p(r)$ is the pair-distance distribution function (PDDF), involving information about the size, shape, and internal core−shell structure of the particles. The intraparticle scattering contribution is called the form factor, $P(q)$, theoretically corresponding to the Fourier transformation of $p(r)$. The interparticle interference scattering is connected to the structure factor, $S(q)$, given as the Fourier transformation of the total correlation function, $h(r) = g(r) - 1$, as

$$S(q) - 1 = 4\pi n \int_0^\infty [g(r) - 1] r^2 \frac{\sin qr}{qr} \mathrm{d}r \quad (2)$$

where n is the particle number density and $g(r)$ is the pair-correlation function.

For monodisperse spherical particle systems, the total scattering, $I(q)$, can simply be given by

$$I(q) = nP(q)S(q) \quad (3)$$

The SAXS data were analyzed by the *generalized indirect Fourier transformation* (GIFT) technique[20,21] with the Boltzmann simplex simulated annealing (BSSA) algorithm, which allows us to determine the form factor and the structure factor simultaneously from the scattering data without any assumption for the form factor, whereas we need appropriate assumptions for the interparticle interaction potential and the closure relation for the structure factor.

Results

Phase Behavior of Water/SDS/$C_{12}EO_n$ Systems. Partial phase diagrams of water/SDS/$C_{12}EO_2$, water/SDS/$C_{12}EO_3$, and water/SDS/$C_{12}EO_4$ systems in the water-rich region at 25 °C are shown in Figure 1. It can be seen that upon adding $C_{12}EO_n$ to the micellar (W_m) solution formed in the binary system at high SDS concentrations, a micellar to hexagonal liquid-crystalline (H_1) phase transformation occurs because $C_{12}EO_n$ compounds penetrate to the palisade layer of the aggregates and reduce their interfacial curvature. It can be seen from the phase diagrams that the H_1 domain intrudes toward the water-rich region, thereby making a bifurcation in the micellar domain. Such an intrusion of the H_1 phase implies that the formation of rodlike aggregates is highly favorable in the particular range of the $C_{12}EO_n$/SDS mixing ratio. When water content is increased at this mixing ratio, the spatial order of the rodlike aggregates observed in the H_1 phase is lost and a viscoelastic solution is formed inside the W_m domain at compositions along the locus starting from the tip of the H_1 domain toward the water corner of the phase diagrams, which is attributed to the formation of very long but flexible cylindrical micelles which entangle to form viscous solutions. These viscoelastic solutions are optically isotropic at rest but birefringent upon shaking. The high-viscosity region inside the W_m domain in the phase diagram of the water/SDS/$C_{12}EO_3$ system is shown by shaded area.

With further addition of $C_{12}EO_n$ to the viscoelastic micellar solutions, an isotropic micellar phase is still observed but the viscosity decreases significantly, and with successive additions of $C_{12}EO_n$, ultimately, a lamellar (L_α) phase separates out beyond the solubilization limit of the W_m phase, whereas at low SDS concentrations, a turbid solution containing vesicular aggregates is formed upon phase separation, which eventually transforms to the lamellar L_α phase at a higher $C_{12}EO_n$ concentration. At a higher SDS concentration, successive

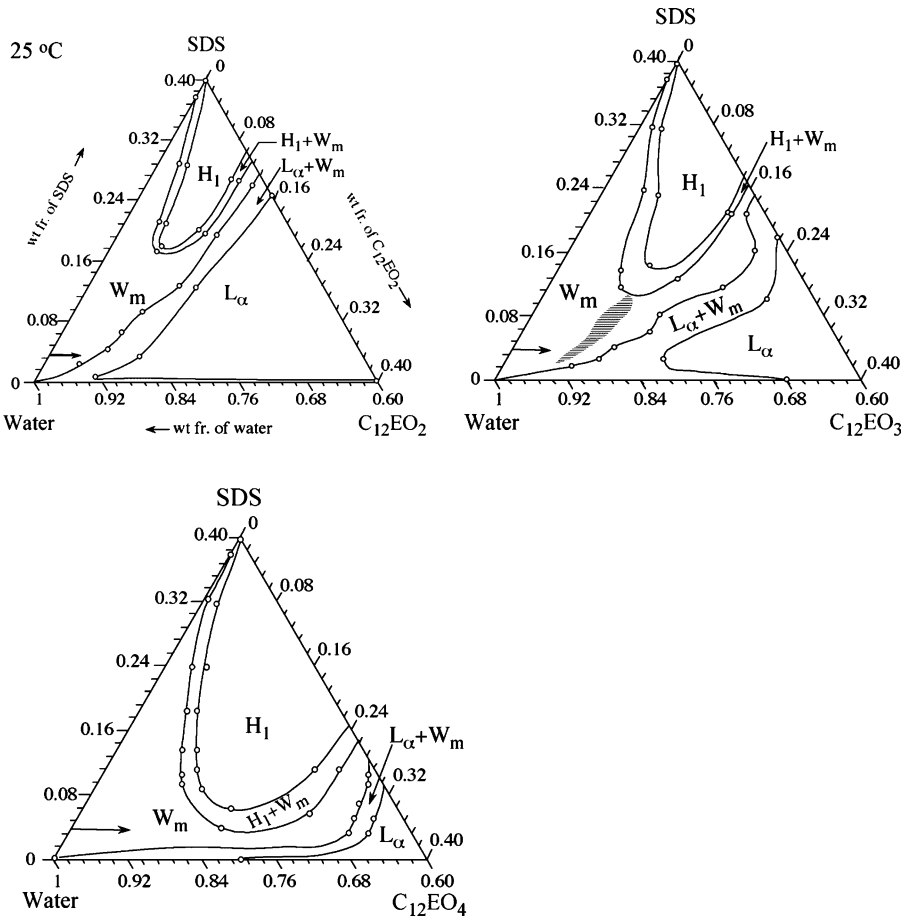

Figure 1. Phase diagrams of water/SDS/$C_{12}EO_n$ systems at 25 °C. W_m is the micellar phase and H_1 and L_α are the hexagonal and lamellar liquid crystalline phases, respectively.

additions of $C_{12}EO_n$ to the H_1 phase induce $H_1-W_m-L_\alpha$ transformation as well. In a closely related system of water/SDS/decanol, an essentially similar pattern of phase behavior has been reported, except that the H_1-L_α phase transition occurs via a narrow domain of columnar and discotic nematic phases successively,[22] which consist of short cylindrical or disklike aggregates with a net orientational order in long range. It is, therefore, reasonable to expect that, with $C_{12}EO_n$, the micellar solution formed between the H_1 and L_α phases in the present systems consists of short, elongated aggregates. The reason for the H_1-W_m transformation or decrease in viscosity of the solution in the micellar solution as mentioned above with increasing $C_{12}EO_n$ concentration is not clearly understood. In fact, the formation of intermediate phases between the H_1 and L_α phases is a result of the contribution of several factors that affect the interfacial curvature of the aggregate.

It can be seen from the phase diagrams that with increasing EO chain length of $C_{12}EO_n$, the domains of the W_m and H_1 phases become wider and the W_m-L_α phase transition shifts to a higher $C_{12}EO_n$ concentration. With a shorter EO chain, the interfacial curvature of the aggregates decreases comparatively swiftly, and therefore, the L_α phase is formed at a lower mixing fraction of the nonionics.

Rheological Behavior. To study the influence of concentration and the EO chain length of $C_{12}EO_n$ on the rheological behavior, several samples were prepared by adding required amounts of $C_{12}EO_n$ to 0.15 M SDS solution (4.32 wt %), along the direction of the arrows shown in the respective phase diagrams. Steady shear-rate−viscosity measurements were performed for these solutions. Figure 2 shows the trend of the evolution of the viscosity curves with increasing concentrations

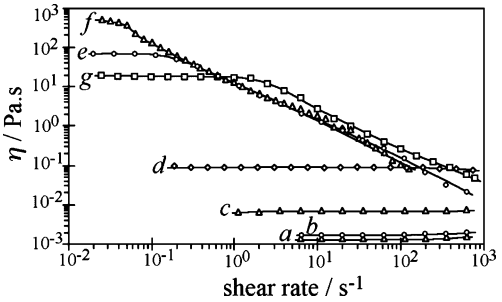

Figure 2. Steady shear-rate−viscosity curves for 0.15 M SDS−$C_{12}EO_3$ systems at different mole fractions of $C_{12}EO_3$ in total surfactant (X): (a) 0, (b) 0.296, (c) 0.456, (d) 0.516, (e) 0.583, (f) 0.616, and (g) 0.643.

of $C_{12}EO_3$ in the system. This trend is similar to that observed for mixed ionic−nonionic surfactant systems.[23−25] At low concentrations of $C_{12}EO_3$, the viscosity is independent of the shear rate, that is, the solutions show Newtonian behavior over the entire range of shear rate studied. With a further increase in $C_{12}EO_3$ concentration, the viscosity increases sharply and a shear thinning is observed at a higher shear rate. This behavior is typical of a wormlike micellar solution because above the critical shear rate the viscosity decreases due to shear alignment of the micelles as well as the breaking of the structured networks. As the $C_{12}EO_3$ concentration increases, the wormlike micelles become more structured and the critical shear rate shifts to lower values, and at $X \sim 0.62$, the sample becomes highly viscoelastic and attains a maximum viscosity (∼500 Pa·s) with no Newtonian region in the entire range of shear rate studied. With a further increase in $C_{12}EO_3$ concentration, the viscosity decreases

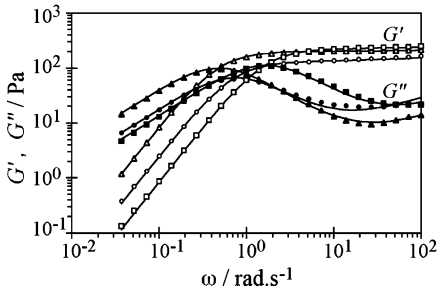

Figure 3. Dynamic rheological behavior for the SDS + $C_{12}EO_3$ system at different mixing fractions of $C_{12}EO_3$, X: 0.594 (○●), 0.609 (▲△), and 0.643 (■□). The lines are the Maxwell plus Rouse combined fitting for the data points.

and the Newtonian region reappears in the low shear-rate region, which corresponds to the structural change in the system. A similar trend was observed with $C_{12}EO_4$, although the maximum viscosity was lower than that with $C_{12}EO_3$.

The viscoelastic behavior in the solutions of wormlike micelles is attributed to the entanglement of the wormlike micelles to form a transient network. When a strain is applied, the stress relaxation occurs by reptation, that is, a reptile-like motion of the micelle along its own contour. Besides this, micelles may undergo reversible scission.[26] When the time scale of the reptation for an average micellar contour length (τ_{rep}) is too long in comparison to the time scale of the scission (τ_{br}), that is, $\tau_{rep} \gg \tau_{br}$, the viscoelastic micellar solutions behave as a Maxwell fluid with a single relaxation time, and variation of the elastic or storage modulus, $G'(\omega)$, and the viscous or loss modulus, $G''(\omega)$, as a function of oscillatory-shear frequency, ω, is described by the following relations

$$G' = G_o \frac{(\omega\tau)^2}{1 + (\omega\tau)^2} \tag{4a}$$

and

$$G'' = G_o \frac{\omega\tau}{1 + (\omega\tau)^2} \tag{4b}$$

where G_o is called the shear (plateau) modulus that is a measure of the degree of entanglements at a given temperature. From the double logarithmic plot of G' and G'' vs ω, the relaxation time, τ, can be estimated as ω_c^{-1}, where ω_c is the crossover frequency, that is, the ω at which $G' = G''$. When the condition $\tau_{rep} \gg \tau_{br}$ is fulfilled, τ is given by $(\tau_{rep} \cdot \tau_{br})^{1/2}$. At low ω values, and $\omega\tau \ll 1$, G' and G'' show different scaling behaviors ($G' \propto \omega^2$ whereas $G'' \propto \omega$) with $G'' > G'$, which corresponds to a liquidlike behavior. For $\omega\tau \gg 1$, that is, at $\omega \gg \omega_c$, G' approaches a constant limiting plateau value equal to G_o, with $G' > G''$ and the system behaves as an elastic material. At $\omega \gg \omega_c$, wormlike micellar systems show an upturn of G'', although the Maxwell equations predict a monotonic decrease. This deviation is thought to have arisen from a transition of the relaxation mode from "slower" reptation to "faster" relaxation modes, namely, the Rouse mode.[26,27]

The results of oscillatory-shear measurements in the viscoelastic samples of SDS + $C_{12}EO_3$ systems are shown in Figure 3. At low shear frequency, the rheological behavior can be described by eqs 4a and 4b which correspond to the existence of single relaxation time, τ. But at a high shear frequency region, G'' does not show a clear minimum but a very wide one followed by an upturn with increasing ω, suggesting a wide spectrum of the stress relaxation or several relaxation processes

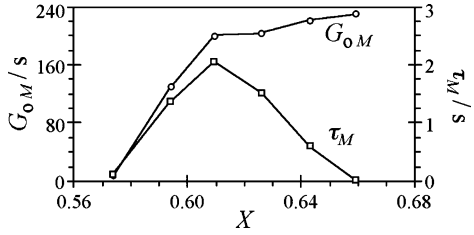

Figure 4. Variation of G_o and τ as a function of the mixing fraction of $C_{12}EO_3$, X, in the 0.15 M SDS−$C_{12}EO_3$ system.

superimposed. If the relaxation mechanism was reptation at long times and Rouse mode at short time (high frequency), the results should be better fitted by eqs 5a and 5b, where a Rouse relaxation mode[28] is combined with the Maxwell equations, the subscripts M and R referring to Maxwell and Rouse relaxations, respectively. The Maxwell plus Rouse fit to the data points is shown by the solid lines in Figure 3.

$$G' = G_{0M} \frac{(\omega\tau_M)^2}{1 + (\omega\tau_M)^2} + G_{0R} \sum_{p=1}^{N} \frac{(\omega\tau_R/p^2)^2}{1 + (\omega\tau_R/p^2)^2} \tag{5a}$$

$$G'' = G_{0M} \frac{\omega\tau_M}{1 + (\omega\tau_M)^2} + G_{0R} \sum_{p=1}^{N} \frac{\omega\tau_R/p^2}{1 + (\omega\tau_R/p^2)^2} \quad (p = 1, 3, 5, ...) \tag{5b}$$

In Figure 4, the variations of G_o and τ, which give information about the easily perceivable physical properties of the transient network, namely, the network density and the length of the wormlike micelles, are plotted as a function of the $C_{12}EO_3$ mixing fraction, X, for the SDS−$C_{12}EO_3$ system. As can be seen from the plot, by increasing the $C_{12}EO_3$ mixing fraction up to $X \sim 0.61$ which is the composition corresponding to the maximum viscosity, both τ and G_o increase, which might have occurred due to a rapid increase in the average counter length of the wormlike aggregates and, consequently, the increase in the number density of the entanglements. With further increase in $C_{12}EO_3$ concentration above $X \sim 0.62$, structural changes occur in the network which is reflected by the change in the variation of the rheological parameters, especially τ. Such a behavior may have originated from the fusion of the free ends of the aggregate with the cylindrical parts of the micelles, thereby forming micellar joints where fast stress relaxation can occur by sliding of the connection point along the cylindrical body.[29]

To study the variation of rheological parameters with total surfactant concentration, rheological measurements were performed at different total concentrations in the SDS + $C_{12}EO_3$ system, keeping the mixing fraction of $C_{12}EO_3$, X, fixed so that the packing properties of the surfactant in the aggregate remain roughly the same. The variation of zero-shear viscosity (η_o) and G_o as a function of the weight fraction of total surfactant is shown in Figure 5. For viscoelastic samples, η_o is calculated from the relation $\eta_o = G_o \cdot \tau$, whereas for less viscous samples it is estimated by extrapolating the steady shear viscosity value to the zero-shear rate. As can be seen in Figure 5, the exponents for each of the power laws are significantly higher than those predicted by the living polymer model of wormlike micelles ($\eta_o \sim f^{3.75}$ and $G_o \sim f^2$, ϕ being the surfactant volume fraction), which takes into account the reptation and reversible scission processes. Although the behavior of wormlike micellar systems of ionic surfactants in the presence of a large concentration of counterions is in close agreement with the theoretical model,[2,6]

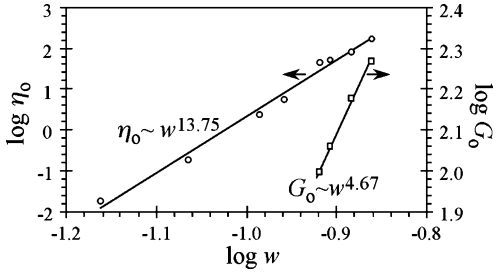

Figure 5. Variation of zero-shear viscosity (η_o) and G_o for SDS−$C_{12}EO_3$ as a function of the weight fraction of total surfactant (w) at a fixed mole fraction of $C_{12}EO_3$ in total surfactant, $X = 0.441$.

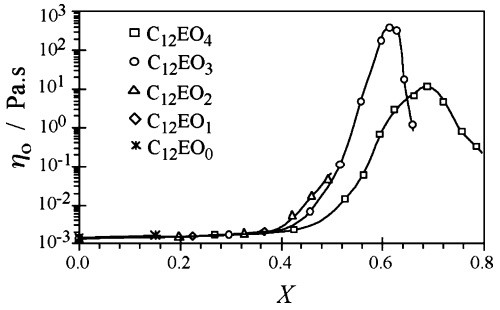

Figure 6. Variation of zero-shear viscosity (η_o) as a function of the mole fraction of $C_{12}EO_n$ in total surfactant, X, for 0.15 M SDS−$C_{12}EO_n$ ($n = 0-4$) systems.

a remarkable deviation from the theoretical model in the present ionic−nonionic surfactant system might have originated from the intermicellar repulsion due to large surface charge density at the micellar surface.

The variation of η_o as a function of the mixing fraction of $C_{12}EO_n$, X, for different 0.15 M SDS−$C_{12}EO_n$ systems is shown in Figure 6. Decreasing the EO chain length from EO_4 to EO_3 increases the extent of micellar growth, with a higher viscosity value occurring at a lower value of X. However, with a further decrease in the EO chain, that is, with $C_{12}EO_2$ and other shorter EO chain amphiphiles, a phase separation occurs at a low value of X.

SAXS Measurement of Micellar Solution. To investigate the effect of $C_{12}EO_n$ addition to the SDS solution on the micellar shape in the mixed systems, SAXS measurements were performed on SDS + $C_{12}EO_n$ micellar solutions at various mixing ratios of the surfactants. The samples were prepared by adding $C_{12}EO_n$ to 0.15 M (∼4.32 wt %) SDS aqueous solutions along the composition line shown by an arrow line in the water-rich corner of the phase diagram (Figure 1b) which is the same as the composition line of the rheological measurements. The precise structure factor ($S(q)$) analysis for charged systems is still a challenging problem for the scattering technique, but at the same time, it is a crucial point for the extraction of the $p(r)$ function. For the GIFT technique, the calculation of $S(q)$ is based on the solutions of the Ornstein−Zernike (OZ) equation[30]

$$h(r) = c(r) + n \int c(\mathbf{r} - \mathbf{r}')h(\mathbf{r}')\, d\mathbf{r}'$$

where the total correlation function, $h(r) = g(r) - 1$, is related to the direct correlation function, $c(r)$, as well as the indirect contributions expressed by the integral term in the OZ equation. In the mean spherical approximation (MSA), $c(r) = -\beta v(r)$, where $\beta = 1/k_BT$ and $v(r)$ describes the particle potential. We calculated the structure factors of the investigated charged systems assuming Yukawa potential for the particle

$$\beta v(r) = \frac{Z^2 e_0^{\,2}}{4\pi\epsilon\epsilon_0 k_B T} \frac{\exp[-\kappa(r-\sigma)]}{r(1+\kappa\sigma/2)^2}$$

where σ is diameter of a particle, Z the charge, ϵ the static dielectric constant of solvent, and κ the reciprocal Debye screening length determined by the ionic strength, with the hypernetted chain (HNC) closure relation[29]

$$g(r) = \exp[-\beta v(r) + h(r) - c(r)]$$

The simulation results showed that it is impossible to determine charge and ionic strength simultaneously, and it has been pointed out that different combinations of the structure factor parameters, volume fraction, charge, and interaction radius, as outputs of the GIFT technique, can give nearly identical shapes of $S(q)$.[30] So even when we consider the screened repulsive interactions for our systems, some ambiguities remain. Nevertheless, with the employed $S(q)$ model, we successfully reproduced all the experimental SAXS curves and extracted the form factor in real space.

Figure 7 shows the scattering functions, $I(q)$, and the corresponding pair-distance distribution functions, $p(r)$, of 0.15 M SDS + $C_{12}EO_3$ systems at different SDS/$C_{12}EO_3$ ratios, as well as the radial electron density profile, $\Delta\rho(r)$, of a SDS micelle in a 0.15 M aqueous solution deconvoluted from its $p(r)$. In Figure 8, we display the $p(r)$ functions of SDS + $C_{12}EO_n$ ($n = 0$, 1, 3, and 4) systems at 1 wt % $C_{12}EO_n$.

The local maximum and minimum in the $p(r)$ function in the low r region come essentially from the productive contribution of the negative and positive electron densities (in comparison to the average value) from the hydrophobic core and hydrophilic shell, respectively, which gives us information about the internal structure of micelles. If we deconvolute the $p(r)$ function of an SDS micelle into the radial electron density distribution profile, $\Delta\rho(r)$, assuming that a SDS micelle at the investigated concentration is nearly spherical, then the distances corresponding to the first inflection point located between the local maximum and minimum in $p(r)$ and the hydrophobic core radius, r_{core}, obtained from $\Delta\rho(r)$ coincide well with each other, giving $r_{core} \sim 1.55$ nm (Figure 7). The second inflection point in $p(r)$ also corresponds to the core diameter. The size of the hydrophilic headgroup, $2r(-OSO_3^-)$, is known to be ∼0.47 nm, so that the maximum diameter of the SDS micelle deduced from $p(r)$, $D_{max} \sim 5.6$ nm, exceeds twice the core radius plus the headgroup size, ∼4.0 nm. One possibility could be that a SDS micelle is already to some extent elongated at 0.15 M. However, it is natural to consider that the counterion cloud on the surface of SDS micelles gives an additional contrast to the SAXS measurement.

According to the solvent-sheared ion-pair (SIP) model for the headgroup hydration, $OSO_3^-(H_2O)Na^+$, suggested by dielectric spectroscopy,[31] if its size of a sulfate headgroup = 0.468 nm, $2r(Na^+) = 0.196$ nm, and $2r(H_2O) = 0.285$ nm are added to the core radius, $r_{core} = 1.55$ nm, deduced from $\rho(r)$, we get the total radius, $R = 2.5$ nm. If the diameter of water is additionally included in the micellar structure, $r_{max} \sim 2.8$ nm is attained and well coincides with r_{max} from $\rho(r)$. If based on the hypothesis that a SDS micelle is spherical, this suggests that the thickness of the conducting surface layer corresponds to the sum of diameters of a counterion (Na^+) and two hydrating water molecules.

An addition of $C_{12}EO_3$ to SDS makes contrast of the SAXS measurement worse. Namely, the forward intensity once becomes weaker by an addition of a small amount of $C_{12}EO_3$.

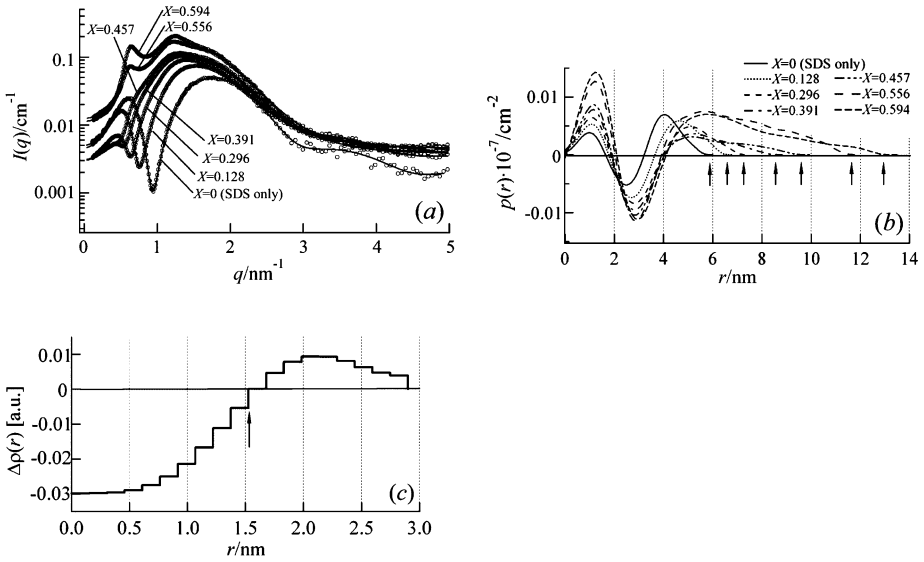

Figure 7. (a) Collimation-calibrated (desmeared) SAXS curves for 0.15 M SDS + $C_{12}EO_3$ systems at different mixing ratios of $C_{12}EO_3$, *X*, obtained on an absolute scale, (b) the corresponding pair-distance distribution functions (PDDFs), $p(r)$, of 0.15 M SDS + $C_{12}EO_3$ systems, and (c) the radial electron density profile for a SDS micelle in 0.15 M aqueous solution, obtained by the deconvolution procedure of $p(r)$ with the help of the program DECON.

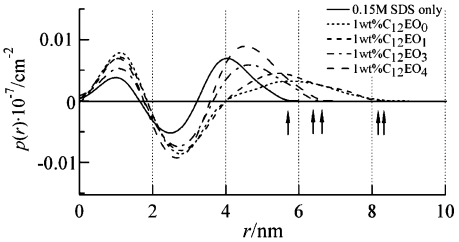

Figure 8. Pair-distance distribution functions (PDDFs) of 0.15 M SDS and 0.15 M SDS + $C_{12}EO_n$ ($n = 0-4$) systems at 1 wt % $C_{12}EO_n$.

Nevertheless, we clearly observed that the scattering functions, $I(q)$, are rapidly shifted toward the low-q side. With a further increase of $C_{12}EO_3$ content, $I(q)$ exhibits a successive shift toward the low-q side and the forward intensity is greatly increased at a high $C_{12}EO_3$ ratio ($X > 0.5$), which makes the effects of the structure factor, the so-called interaction peak(s), clearly visible on the scattering functions at $q \sim 0.65$ nm^{-1}. Directly associated with such a characteristic concentration dependence of $I(q)$, D_{max} of $p(r)$, extracted by the GIFT analysis, is rapidly increased with increasing $C_{12}EO_3$ content.

The deconvolution procedure of $p(r)$ into $\Delta\rho(r)$ requires a precondition of the homogeneous orientation (spherical symmetry) and is not valid for elongated structures. However, it is recently pointed out that the second inflection point, r_2, in $p(r)$ after the local minimum can be a good measure for the approximate size of the hydrophobic core diameter also for the elongated (rodlike) structure even when the maximum size of the aggregates exceeds the maximum resolution of the scattering measurements. Additionally, we have found that the first inflection point, r_1, in $p(r)$ seen between the local maximum and minimum is always approximately two times shorter than r_2. The position of the first and second inflections in the $p(r)$ functions for SDS−$C_{12}EO_3$ micelles are virtually unchanged despite the increasing $C_{12}EO_3$ content in the systems (Figure 8). This indicates a nearly constant core diameter despite large variations in the SDS/$C_{12}EO_3$ ratio. Our findings, virtually constant core diameter, rapid growth of the maximum size of micelles with increasing $C_{12}EO_3$ content, and linearly decaying tail of $p(r)$ curve at high r region in Figure 7b give direct evidence that the micellar growth is 1D. If the 2D growth of the micelle would have taken place, then the core radius should have shrunk considerably. Because all the surfactant molecules would be in an extended state if the bilayer distance of the disklike micelle is the same as the diameter of the spherical micelles, it is not possible in the liquid state. This is the same situation as hexagonal and lamellar liquid crystals. In the H_1 phase (cylindrical aggregates), the micellar radius of cross-section is almost similar to the hydrocarbon chain in its extended state. It means that only a few surfactant molecules are really in the extended state. On the other hand, in the lamellar phase, the half thickness of the bilayer is considerably shorter than the surfactant molecule in the extended state. Because surfactant molecules in lamellar phase are in a liquid state, it is not possible that all the molecules are in the extended state.

Summary

Upon the addition of short EO chain $C_{12}EO_n$ to dilute micellar solution of SDS above a particular concentration, a sharp increase in viscosity occurs and a highly viscoelastic micellar solution is formed. At higher SDS concentration, the addition of $C_{12}EO_n$ above the solubilization limit of the H_1 phase induces H_1-L_α phase transition. In the phase diagram, the region of viscoelastic micellar regaion is located near the apex of the H_1 domain, stretched toward the water-rich region. The oscillatory-shear rheological behavior of the viscoselastic solutions can be described by the Maxwell model at low shear frequency and combined Maxwell−Rouse model at high shear frequency. This property is typical of wormlike micelles entangled to form a transient network. It is found that when $C_{12}EO_4$ in the mixed system is replaced by $C_{12}EO_3$ the micellar growth occurs more effectively. However, with very short EO chain length, phase separation occurs before a viscoelastic solution is formed. SAXS measurement gives direct evidences of a sphere−rod transition in micellar shape and 1D micellar growth induced by $C_{12}EO_n$ in SDS micelles. Consistent with the results of rheological measurement, SAXS measurements show that increasing $C_{12}EO_n$/SDS mixing ratios favor micellar growth and also that the shorter the EO chain length in $C_{12}EO_n$ the greater the tendency of 1D micellar growth.

Acknowledgment. The authors appreciate the technical assistance of Koheita Hattori and Noriko Ishii during the

experiment. D.P.A. thanks the Japan Society for the Promotion of Science (JSPS) for financial support.

References and Notes

(1) Rehage, H.; Hoffmann, H. *J. Phys. Chem.* **1988**, *92*, 4712−4719.
(2) Kern, F.; Lemarechal, P.; Candau, S. J.; Cates, M. E. *Langmuir* **1992**, *8*, 437−440.
(3) Clausen, T. M.; Vinson, P. K.; Minter, J. R.; Davis, H. T.; Talmon, Y.; Miller, W. G. *J. Phys. Chem.* **1992**, *96*, 474−484.
(4) Khatory, A.; Kern, F.; Lequeux, F.; Appell, J.; Porte, G.; Morie, N.; Ott, A.; Urbach, W. *Langmuir* **1993**, *9*, 933−939.
(5) Khatory, A.; Lequeux, F.; Kern, F.; Candau, S. J. *Langmuir* **1993**, *9*, 1456−1464.
(6) Berret, J.-F.; Appell, J.; Porte, G. *Langmuir* **1993**, *9*, 2851−2854.
(7) Lin, Z.; Cai, J. J.; Scriven, L. E.; Davis, H. T. *J. Phys. Chem.* **1994**, *98*, 5984−5993.
(8) Koehler, R. D.; Raghavan, S. R.; Kaler, E. W. *J. Phys. Chem. B* **2000**, *104*, 11035−11044.
(9) Raghavan, S. R.; Fritz, G.; Kaler, E. W. *Langmuir* **2002**, *18*, 3797−3803.
(10) Kato, T.; Terao, T.; Seimiya, T. *Langmuir* **1994**, *10*, 4468−4474.
(11) Schurtenberger, P.; Cavaco, C.; Tiberg, F.; Regev, O. *Langmuir* **1996**, *12*, 2894−2899.
(12) Acharya, D. P.; Hattori, K.; Sakai, T.; Kunieda, H. *Langmuir* **2003**, *19*, 9173−9178.
(13) Rodriguez, C.; Acharya, D. P.; Maestro, A.; Hattori, K.; Kunieda, H. *J. Chem. Eng. Jpn.* **2004**, *37*, 622−629.
(14) Rodriguez, C.; Acharya, D. P.; Hattori, K.; Sakai, T.; Kunieda, H. *Langmuir* **2003**, *19*, 8692−8696.
(15) Herb, C. A.; Chen, L. B.; Sun, W. M. In *Structure and Flow in Surfactant Solutions*; Herb, C. A., Prud'homme, R. K., Eds.; ACS Symposium Series 578; American Chemical Society: Washington, D.C., 1994; pp 153−166.
(16) Acharya, D. P.; Kunieda, H. *J. Phys. Chem. B* **2003**, *107*, 10168−10175.
(17) Acharya, D.; Hossain, Md. K.; Jin-Feng, Sakai, T.; Kunieda H. *Phys. Chem. Chem. Phys.* **2004**, *6*, 1627−1631.
(18) Acharya, D.; Shiba, Y.; Aratani, K.-i. Kunieda, H. *J. Phys. Chem. B* **2004**, *108*, 1790−1797.
(19) Maestro, A.; Acharya, D. P.; Furukawa, H.; Gutiérrez, J. M. López-Quintela, M. A.; Ishitobi, M.; Kunieda, H. *J. Phys. Chem. B* **2004**, *108*, 14009−14016.
(20) Brunner-Popela, J.; Glatter, O. *J. Appl. Crystallogr.* **1997**, *30*, 431−442.
(21) Weyerich, B.; Brunner-Popela, J.; Glatter, O. *J. Appl. Crystallogr.* **1999**, *32*, 197−209.
(22) Quist, P.-O. *J. Phys. Chem.* **1996**, *100*, 4976−4987.
(23) Acharya, D. P.; Hattori, K.; Sakai, T.; Kunieda, H. *Langmuir* **2003**, *19*, 9173−9178.
(24) Rodriguez, C.; Acharya, D. P.; Hattori, K.; Sakai, T.; Kunieda, H. *Langmuir* **2003**, *19*, 8692−8696.
(25) Rodriguez, C.; Acharya, D. P.; Maestro, A.; Hattori, K.; Kunieda, H. *J. Chem. Eng. Jpn.* **2004**, *37*, 622−629.
(26) Granek, R.; Cates, M. E. *J. Chem. Phys.* **1992**, *96*, 4758−4767.
(27) Doi, M.; Edwards, S. F. *The Theory of Polymer Dynamics*; Oxford University Press: Clarendon, U.K., 1986.
(28) Rouse, P. E. J. *J. Chem. Phys.* **1953**, *21*, 1272−1280.
(29) Candau, S. J.; Oda, R. *Colloid Surf., A* **2001**, *183−185*, 5−14.
(30) Fritz, G.; Bergmann, A.; Glatter, O. *J. Chem. Phys.* **2000**, *113*, 9733−9740.
(31) Fernandez, P.; Schrödle, S.; Buchner, R.; Kunz, W. *ChemPhysChem* **2003**, *4*, 1065−1072.